VERIFICATION OF TURBULENCE AND NON-DRAG INTERFACIAL FORCE MODELS OF A COMPUTATIONAL MULTI-FLUID DYNAMICS CODE

Ik Kyu Park[*1] and Kun Ho Chun[2]
[1]Korea Atomic Energy Research Institute
[2]KEPCO Nuclear Fuel

CMFD 코드의 난류 모델 및 비견인력 모델의 검증 계산

박 익 규,[*1] 전 건 호[2]
[1]한국원자력연구원
[2]한전원자력연료㈜

The standard drag force and virtual mass force, which exert to the primary flow direction, are generally considered in two-phase analysis computational codes. In this paper, the lift force, wall lubrication force, and turbulent dispersion force including turbulence models, which are essential for a computational multi-fluid dynamics model and play an important role in motion perpendicular to the primary flow direction, were introduced and verified with conceptual problems.

Key Words : Turbulence model, Lift force, Wall lubrication force, Turbulent dispersion force, CUPID code

Nomenclature

c_p : Specific heat [J/kg]
C : Proportional coefficient [1]
d, D : Diameter [m]
e : Internal energy [J/kg]
g : Gravity acceleration [m/s^2]
F : Force term [$kg/m^3/s$]
h : Enthalpy [J/kg]
I : Interfacial energy transfer rate [$J/m^3/s$]
M : Interfacial momentum transfer term [$kg/m^2/s^2$]
n : Normal surface vector of wall [m]
u, U : Velocity [m/s]
p, P : Pressure [Pa]
Pr : Prandtl number [1]
Re : Reynolds number [1]
r : Radius [m]
Sc : Schmidt number [1]
St : Stokes number [1]
t : Time [s]
T : Temperature [K]
y : Distance from wall [m]

Greek Letter
α : Volume fraction [1]
Γ : Interfacial mass transfer rate [$kg/m^3/s$]
κ : Von Karman constant [1]
μ : Viscosity [$N \cdot s/m^2$]
ν : Kinematic viscosity [m^2/s]
ρ : Density [kg/m^3]
σ : Surface tension [N/m]
$\sigma_k, \sigma_\varepsilon$: Turbulent Prandtl number [1]
τ : Shear stress [N/m^2]

Subscripts, Superscripts
b : Bubble

Received: May 20, 2013, Revised: June 18, 2013, Accepted: June 18, 2013.
* Corresponding author, E-mail: gosu@kaeri.re.kr
DOI http://dx.doi.org/10.6112/kscfe.2013.18.2.099

D : Drag
eff : Effective
g : Gas
i : Interface
k : $=g,l \text{ or } d$
l : Liquid
L : Lift
m : Mixture
t : Tangential
T : Turbulence
TD : Turbulent dispersion
w : Wall
WL : Wall lubrication

1. Introduction

A computational multi-fluid dynamics (CMFD) code, CUPID has been developed for a transient three-dimensional two-phase flow analysis of nuclear reactor components[1,2,3]. The semi-implicit ICE scheme used in the RELAP5 code[4] was adopted as a basic numerical method, which uses a staggered grid and a donor-cell scheme. The main advantages of this scheme are its computational efficiency and robustness.

In this numerical scheme, the momentum equations are solved first to represent each phasic velocity at a cell face as a function of the pressure difference of the adjacent cells. The mass and energy equations are coupled, and with some algebraic operations, reduced to a cell pressure equation that includes unknown pressures of the computational cell and its adjacent cells. Finally, a system pressure equation is established and solved. The phasic velocities at the junctions are obtained by a back-substitution. However, to apply this scheme with an unstructured finite volume method, this scheme should be changed to adopt a cell-centered scheme. For this, the momentum equations were solved over a non-staggered grid, and the velocities at the cell faces were interpolated using the Rhie-Chow scheme[5].

The CUPID code is based on a two-fluid, three-field model, which is solved using an unstructured finite volume method. The three fields in the CUPID code represent a continuous liquid, an entrained liquid, and a vapor field. To describe the interfacial and relative motion between phases, the momentum equations for each phase included the momentum transfer owing to the phase change, generalized interfacial drag force, and virtual mass force.

In the two phase flow momentum equation, the most important term to be modeled by a constitutive relation is the generalized drag force that specifies the interfacial surface forces. This force can be formulated as the linear combination of various known interfacial forces as the sum of the standard drag force, lift force, wall lubrication force, turbulence dispersion force, and so on[6]. The lift force, wall lubrication force, and turbulent dispersion force are known to affect the void fraction of the normal direction of the primary flow direction.

As a computational multi-fluid dynamics code for a two-phase flow, the CUPID code needs to be tested for its justification, and thus some verification calculations were conducted over several sample problems[1,2,3]. In this paper, implementations and verifications of the turbulence, lift force, wall lubrication force, and turbulence dispersion force models to extend the capability of the CUPID code were discussed.

2. Mathematical model

2.1 Governing equations

The governing equations of the two-fluid, three-field model are similar to those of the time-averaged two-fluid model derived by Ishii and Hibiki[7]. The continuity, momentum, and energy equations for the k-phase are given by

$$\frac{\partial}{\partial t}(\alpha_k \rho_k) + \nabla \cdot (\alpha_k \rho_k \underline{u}_k) = \Gamma_k \tag{1}$$

$$\begin{aligned}\frac{\partial(\alpha_k \rho_k \underline{u}_k)}{\partial t} + \nabla \cdot (\alpha_k \rho_k \underline{u}_k \underline{u}_k) &= -\alpha_k \nabla P \\ &+ \nabla \cdot [\alpha_k \tau_k] + \alpha_k \rho_k \underline{g} + M_k^{mass} + M_k^{drag} \\ &+ M_k^{VM} + M_k^{non-drag}\end{aligned} \tag{2}$$

$$\begin{aligned}\frac{\partial(\alpha_k \rho_k e_k)}{\partial t} + \nabla \cdot (\alpha_k \rho_k e_k \underline{u}_k) &= \nabla \cdot \left(\alpha_k q_k\right) \\ &- P \frac{\partial}{\partial t} \alpha_k - P \nabla \cdot (\alpha_k \underline{u}_k) + I_k + Q'''_k\end{aligned} \tag{3}$$

where, $\alpha_k, \rho_k, u_k, P, \Gamma_k$, and I_k are the k-phase volume fraction, density, velocity, pressure, and interfacial mass transfer rate, and interfacial energy transfer rate, respectively. M_k represents the interfacial momentum transfer owing to a mass exchange, standard drag force,

and several drag forces except the standard drag force virtual mass. $M_k^{non-drag}$ includes the lift force (M_k^L), wall lubrication force (M_k^{WL}), and turbulence dispersion force (M_k^{TD}).

$$M_k^{mass} = \sum_{j}^{j\neq k} \Gamma_{j\to k}\underline{u}_j - \sum_{j}^{j\neq k} \Gamma_{k\to j}\underline{u}_k \tag{4}$$

$$M_k^{drag} = \sum_{i}^{i\neq k} F_{ik}\left(\underline{u}_i - \underline{u}_k\right) \tag{5}$$

$$M_k^{VM} = \sum_{i}^{i\neq k} C_{ik}\alpha_i\alpha_k\rho_{m,ik}\frac{\partial\left(\underline{u}_i - \underline{u}_k\right)}{\partial t} \tag{6}$$

$$M_k^{non-drag} = M_k^L + M_k^{WL} + M_k^{TD} \tag{7}$$

M_k^L, M_k^{WL} and M_k^{TD} will be discussed in the following section. Further detailed two-phase flow mathematical descriptions are given in Ref.[7]. For a closure of the system of equations, constitutive relations and the equations of the states are included.

2.2 Turbulence model

The averaging procedure for the momentum equation introduces additional unknown terms containing products of the fluctuating quantities, which act like additional stresses in a fluid. These terms, called 'turbulent' or 'Reynolds' stresses, are difficult to determine directly and thus become further unknowns. With eddy viscosity turbulence models, the shear stress term can be explained by

$$\tau_k = \mu_{k,eff}\left[\nabla\underline{u}_k + \left(\nabla\underline{u}_k\right)^T\right] \tag{8}$$

where μ_{eff} is the effective viscosity defined by the sum of the molecular viscosity and turbulent viscosity.

$$\mu_{k,eff} = \mu_k + \mu_{k,T} \tag{9}$$

A very simple eddy viscosity model computes a global value for $\mu_{k,T}$ from the mean velocity and geometric length scale using an empirical formula. Because no additional transport equations are solved, these models are termed 'zero equation':

$$\mu_{k,T} = \rho_k C_\mu U_k l_T \tag{10}$$

where C_μ is a proportional constant. The velocity scale can be taken to be the maximum velocity in the fluid domain. The length scale is derived using the formula as follows:

$$l_T = \left(V_D{}^{1/3}\right)/7 \tag{11}$$

where V_D is the fluid domain volume.

For the physical meaningful calculation, the $k-\varepsilon$ turbulence model was also implemented. The effective viscosity of the continuous liquid phase is the sum of the laminar viscosity, turbulence viscosity, and bubble effect. The effective viscosity of the dispersed gas phase can be calculated by assuming the same kinematic viscosity of the liquid and gas.

$$\mu_{l,eff} = \mu_l + \mu_{l,T} + \mu_{b,T} \tag{12}$$

$$\mu_{l,T} = C_\mu\rho_l\frac{k_l^2}{\varepsilon_l} \tag{13}$$

$$\mu_{b,T} = 0.6d_b\alpha_g\left|\underline{u}_g - \underline{u}_l\right| \tag{14}$$

$$\mu_{g,eff} = \mu_{l,eff}\frac{\rho_g}{\rho_l} \tag{15}$$

The $k-\varepsilon$ transport equations are established for continuous liquid phase as follows:

$$\frac{\partial\left(\alpha_l\rho_l k_l\right)}{\partial t} + \nabla\cdot\left(\alpha_l\rho_l k_l\underline{u}_l\right) = \nabla\cdot\left[\alpha_l\left(\mu + \frac{\mu_T}{\sigma_k}\right)_l\nabla k\right] + \alpha_l P_k - \alpha_l\rho_l\varepsilon \tag{16}$$

$$\frac{\partial\left(\alpha_l\rho_l\varepsilon_l\right)}{\partial t} + \nabla\cdot\left(\alpha_l\rho_l\varepsilon_l\underline{u}_l\right) = \nabla\cdot\left[\alpha_l\left(\mu + \frac{\mu_t}{\sigma_k}\right)_l\nabla\varepsilon_l\right] + \frac{\alpha_l\varepsilon_l}{k_l}\left(C_{\varepsilon 1}P_k - C_{\varepsilon 2}\rho_l\varepsilon_l\right) \tag{17}$$

$$P_k = \mu_T\left(\nabla\underline{u}_l + \nabla^T\underline{u}_l\right):\nabla\underline{u}_l \tag{18}$$

where $C_\mu, \sigma_\varepsilon, \sigma_k, C_{\varepsilon 1}$, and $C_{\varepsilon 2}$ are recommended to

have a value of 0.09, 1.3, 1.0, 1.44, and 1.92 in the standard $k-\varepsilon$ model, respectively.

Algebraic turbulence models or zero-equation turbulence models are models that do not require the solution of any additional equations, and are calculated directly from the flow variables. As a consequence, zero equation models may not be able to properly account for the unsteady transport of the turbulence, such as the convection and diffusion of turbulent energy. These models are often too simple for use in general situations, but can be quite useful for simpler flow geometries or in start-up situations. A more complicated model may have difficulty in the initial phases of computation because the transport models needs guessing initial values properly and are affected by the fluctuating startup velocity field in the transient calculations.

The wall-function in the CUPID code is an extension of the method of Launder and Spalding[8]. In the log-law region, the near wall tangential velocity is related to the wall-shear-stress by means of a logarithmic relation. In the wall-function approach, the viscosity affected sublayer region is bridged by employing empirical formulas to provide near-wall boundary conditions for the mean flow and turbulence transport equations. The logarithmic relation for the near wall velocity is given by.

$$u^+ = \frac{U_t}{u_\tau} = \frac{1}{\kappa}\ln\left(Cy^+\right) = \frac{1}{\kappa}\ln\left(C\frac{\rho\Delta y u_\tau}{\mu}\right) \tag{19}$$

where $u^+, u_\tau, U_t, y^+, \kappa$, and C are the dimensionless velocity, friction velocity, near wall tangential velocity known velocity tangent to the wall at a distance of Δy from the wall, dimensionless distance from the wall, von Karman constant, and constant depending on the wall roughness.

A wall-function simulation normally requires that y^+ of the first cell outside the walls is in the log-layer, which starts at about $y^+ = 20$, and depending on the Reynolds number, extends up to say $y^+ = 200$.

2.3 LIFT FORCE MODEL

In the context of a fluid flow relative to a body, the lift force is the component of the aerodynamic force perpendicular to the flow direction. This contrasts with the drag force, which is the parallel component of the aerodynamic force. Lift is commonly associated with the wing of an aircraft, although lift is also generated by rotors on helicopters, sails and keels on sailboats, hydrofoils, wings on auto racing cars, and wind turbines. While the common meaning of the word "lift" suggests that the lift opposes gravity, aerodynamic lift can be in any direction. When an aircraft is cruising, for example, the lift opposes gravity.

While a single particle moving through a very viscous liquid relative to a uniform simple shear, the particle experiences a lift force perpendicular to the flow direction[9]. In the two-phase flow, the lift force is commonly associated with a bubble. The lift force represents the interaction of the bubble with the shear field of the liquid. The velocity differences between the bubble and liquid are asymmetric, and thus the pressure on the bubble surface is also asymmetric while the bubble is moving in a viscous liquid. This asymmetric pressure distribution on the bubble surface results in the lift force acting on the bubble. This force pushes the bubble perpendicular to the liquid motion. The lift force is given in terms of the slip velocity and curl of the continuous phase velocity by

$$M_l^L = \alpha_g \rho_l C_L \left(\underline{u}_g - \underline{u}_l\right) \otimes \left(\nabla \otimes \underline{u}_l\right) \tag{20}$$

The classical lift force for bubbles has a positive coefficient, and acts in the direction of decreasing liquid velocity[10]. This force pushes the bubbles toward the pipe wall in the case of a concurrent upward pipe flow. Numerical and experimental investigations showed that the direction of the lift force changes its sign depending on the substantial deformation of the bubble. Tomiyama studied single bubbles in a well-defined shear field and derived the following correlation for the coefficient of the lift force from the experiments[11,12].

$$C_L = \begin{Bmatrix} \min\left[0.288\tanh\left(0.121\mathrm{Re}_{bub}\right), f\left(E_o\right)\right]; E_o < 4 \\ -0.29; E_o > 10 \\ f\left(E_o\right) = .00105E_o^3 - .0159E_o^2 - .0204E_o + .474 \end{Bmatrix} \tag{21}$$

The Reynolds number of particles is defined as follows:

$$\mathrm{Re}_b = \frac{\rho_l \left|\underline{u}_b - \underline{u}_l\right| d_b}{\mu_l} \tag{22}$$

The coefficient, C_L, depends on the modified Eötvös

number given by

$$E_o = \frac{g(\rho_l - \rho_g)d_H^2}{\sigma} \tag{23}$$

where d_H is the maximum horizontal dimension of the bubble. It is calculated using an empirical correlation for the aspect ratio by Wellek et al. from the following equation[13].

$$d_H = d_b\left(1 + 0.163Eo^{0.757}\right)^{1/3} \tag{24}$$

For the water-air system at normal conditions, C_L changes its sign at a bubble diameter of d_b = 5.8 mm[11,12].

In this paper, C_L was set to be 0.01, and the sophisticated formulation of C_L including the change in direction will be discussed later.

2.4 Wall lubrication force model

The gas fraction distribution in the near wall region is important for the general flow structure in the case of the pipe flow. It is mainly determined by the lift and wall forces. Antal et al.[14] proposed a wall lubrication force as follows:

$$F_{WL} = -\frac{\rho_l \alpha_g}{r_b}\left(C_1 - C_2\left(\frac{r_b}{y}\right)\right)u_{rel}^2 \vec{n}_w \tag{25}$$

with $C_1 = -0.104 - 0.06u_{rel}$ and $C_2 = 0.147$.

Tomiyama modified this approach for a special case of a pipe flow as follows[11]:

$$M_l^{WL} = -C_{WL} r_b \alpha_g \left(\frac{1}{y^2} - \frac{1}{(d_b - y)^2}\right)\rho_l u_{rel}^2 \vec{n}_w \tag{26}$$

The coefficient was determined in experiments on single air bubbles in a glycerol solution as follows[14]:

$$C_{WL} = \begin{cases} \exp(-0.933E_o + 0.179); 1 \le E_o \le 5 \\ 0.007E_o + 0.04; 5 \le E_o \le 33 \end{cases} \tag{27}$$

In this paper, a similar correlation by Antal et al. is tested as

$$M_l^{WL} = \frac{\alpha_g \rho_l C_L \left|\underline{u}_g - \underline{u}_l\right|^2}{d_b} \max\left(0, C_1 + C_2 \frac{d_b}{y_w}\right)\vec{n} \tag{28}$$

with C_1 = -0.01 and C_2 = 0.05. The wall lubrication force is limited within $y_w < 5d_b$ in this formulation. A more sophisticated model such as that in Eq. (26) will be discussed later.

2.5 Turbulence dispersion force model

The turbulent dispersion force is the result of the turbulent fluctuations of the liquid velocity. Lahey et al. derived an equation for the force per unit of volume as follows[15,16]:

$$F_{TD,l} = -C_{TD}\rho_l k_l \nabla \alpha_l \tag{29}$$

with a coefficient C_{TD} set to 0.1. A more generalized non-uniform turbulent dispersion coefficient on the basis of homogeneous turbulence was proposed by Lopez de Bertodano[17]. It depends on the Stokes number as follows:

$$C_{TD} = C_\mu^{1/4} \frac{1}{S_t(1 + S_t)} \tag{30}$$

Gosman et al. derived a turbulent dispersion force as follows[18] :

$$F_{TD} = -\frac{3}{4}\frac{C_D \nu_{T,l}}{d_{bubble}\,\mathrm{Pr}_T}\rho_l U_{rel} \nabla \alpha_l \tag{31}$$

The turbulent Prandtl number (Pr_T), has an order of magnitude of 1 and is given by

$$\mathrm{Pr}_T = \frac{\nu_{l,eff}}{\nu_g} \tag{32}$$

Recently, Burns et al. suggested the model for the turbulence dispersion force as follows[19]:

$$F_{TD} = C_{TD} C_D \frac{\nu_{T,g}}{Sc_{T,g}}\left(\frac{\nabla \alpha_l}{\alpha_l} - \frac{\nabla \alpha_g}{\alpha_g}\right) \tag{33}$$

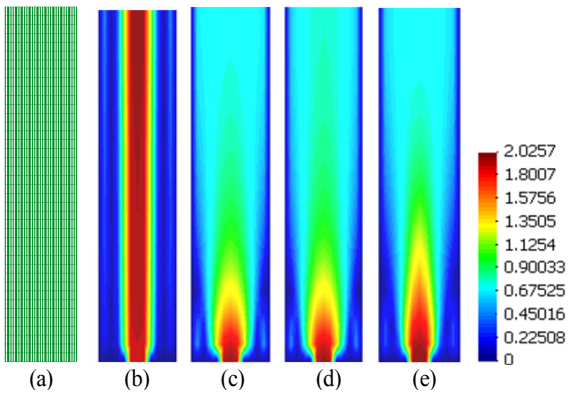

Fig. 1 Effect of turbulence models: (a) meshes, (b) laminar, (c) zero eq. model without wall function, (d) zero eq. model, (e) $k-\varepsilon$ model

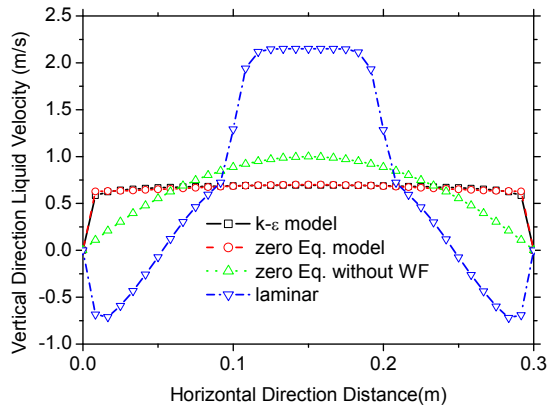

Fig. 2 Vertical velocity distribution at the exit for various turbulence models

where C_{TD}, C_D, $\nu_{T,g}$ and $Sc_{T,g}$ are the turbulent dispersion coefficient (~1), drag coefficient (~2), turbulent kinematic viscosity for gas, and turbulent Schmidt number for gas (~0.9).

In this paper, the turbulence dispersion force model by Burns et al. was used, but it becomes singular when α_g = 0 or α_1 = 0, which can occur in a subcooled boiling flow. Thus, the turbulence dispersion force model by Lahey et al. seems to be a general formulation for the boiling water flow. The non-drag forces for the gas phase has the same magnitude and opposite sign as follows:

$$M_g^{non-drag} = -M_l^{non-drag} \tag{34}$$

3. Qualitative verification

3.1 Verification of turbulence model

A 2-dimensional single phase flow was simulated for a verification of the implemented turbulence model and wall-function. A single-phase upward flow of 2 m/s was assumed in a vertical tube 4 m long and 0.3 m wide. The diameter of the bottom inlet is 0.1 m, and the diameter of the upper outlet is 0.3 m, which is the same as the width of the tube.

As shown in Fig. 1, 1440 (36 x 40) cells are used for this calculation. Three cases were defined as case A without a zero-equation and wall-function, case B with only a zero-equation, case C with a zero-equation and wall-function, and case D with the $k-\varepsilon$ turbulence model and wall-function.

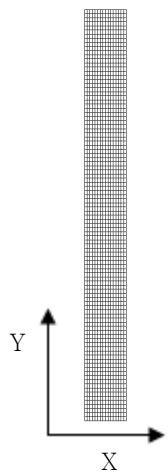

Fig. 3 2-dimensional duct of 0.4 m x 40 m for verification calculation of $k-\varepsilon$ model

The velocity contours are presented in Fig. 1, and the velocity profiles at the exit are presented in Fig. 2. The flow velocities are not developed over the entire tube for case A because the Reynolds number is very high, but the turbulence model is not used. In case B, the flow velocities are developed just like a fully developed laminar velocity profile. In cases C and D, the flow velocities are developed, and the flow looks like a prototypical turbulent flow.

2-dimensional duct of 0.4 m x 4m, of which the bottom and top are the inlet and outlet, was considered as the verification calculation domain for a $k-\varepsilon$ turbulence model. As shown in Fig. 3, 1600 (16 x 100) cells are

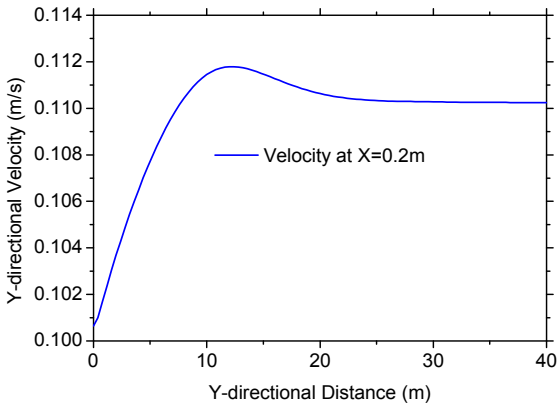

Fig. 4 Vertical velocity along the axial center line

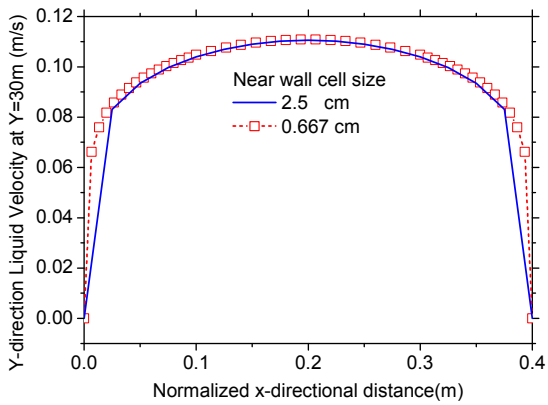

Fig. 6 Vertical velocity at 3/4 of solution domain, 30 m from the bottom inlet

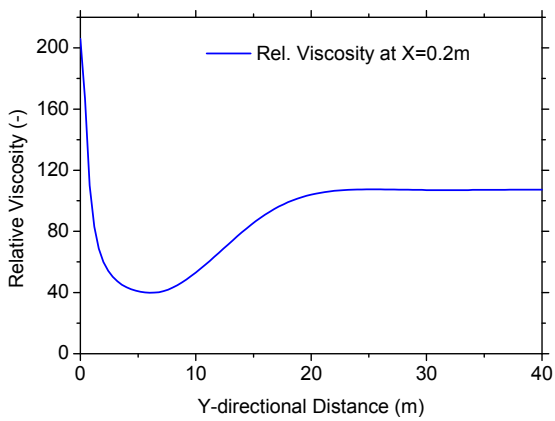

Fig. 5 Relative viscosity along the axial center line

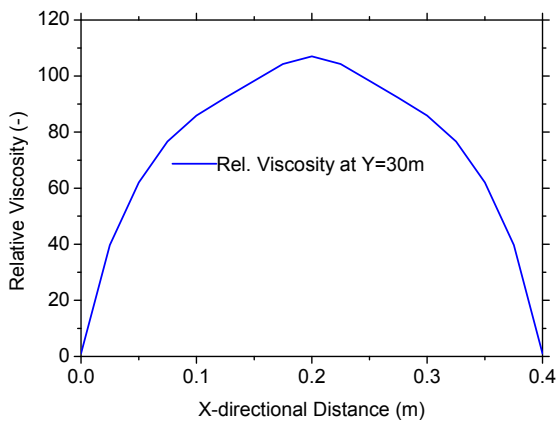

Fig. 7 Relative viscosity at 3/4 of solution domain, 30 m from the bottom inlet

used for this calculation. The 20°C water comes in with 0.1 m/s through the inlet. The pressure of the domain is 0.1 MPa, and the density and viscosity are 998 kg/m^3 and 0.001 $N \cdot s / m^2$. Thus, the L/D is 100, and the Reynolds number is about 40,000.

A steady state solution was obtained using a null-transient calculation. The velocity and relative viscosity profiles are presented in Figs. 4 and 5. The velocity and relative viscosity reach a steady state at 2/3 of the solution domain, 25 m from the bottom inlet. The vertical velocity and relative viscosity at 3/4 of the solution domain, 30 m from the bottom inlet are presented in Figs. 6 and 7.

In Fig. 8, the calculated $u^+(y^+)$ was compared to the analytical wall function as follows:

$$u^+ = \frac{1}{0.41}\ln(y^+) + 5.5 \tag{35}$$

The calculated friction velocity was compared to the wall friction velocity from the Moody chart[20]. The friction velocity of a pipe flow can be obtained as follows:

$$u_\tau = V\left(\frac{f}{8}\right)^{\frac{1}{2}} \tag{36}$$

The friction velocity in the Moody chart is 0.0052 m/s when the Reynolds number is 40,000 and the fraction factor (f) is 0.033. In the calculation, the friction

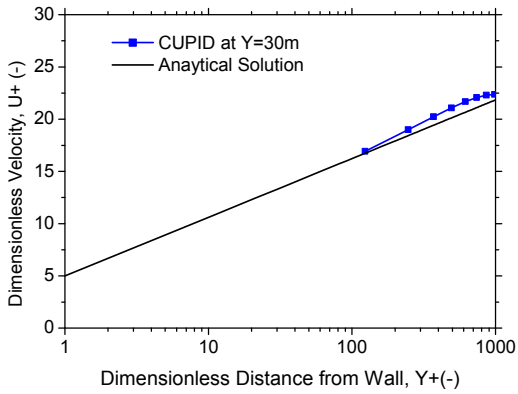

Fig. 8 Comparison to the wall function

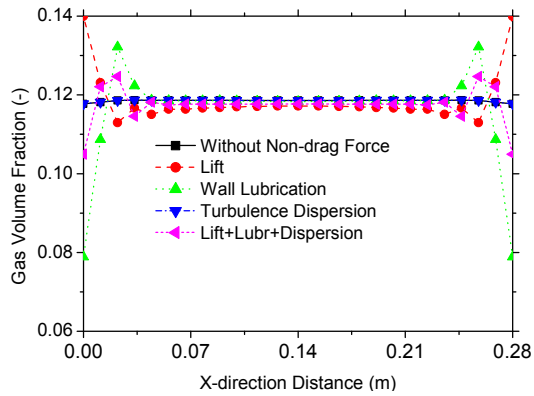

Fig. 10 Void fraction distribution at the exit

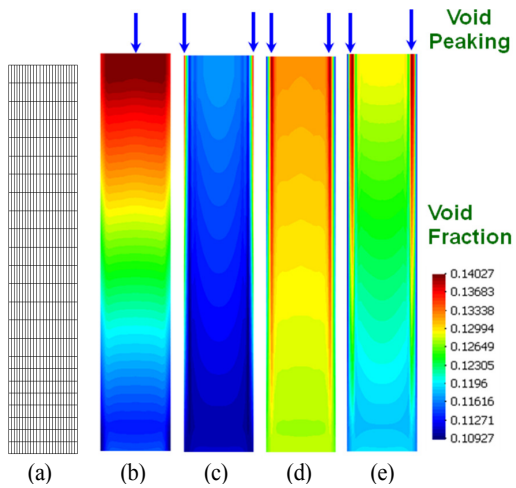

Fig. 9 Void fraction contour for the non-drag force: (a) meshes, (b) only lift, (c) only wall lubrication, (d) wall lubrication, (e) all non-drag forces (↓ indicates the radial location of a void peak)

velocity is 0.0049 m/s, and the error from the Moody chart value is 5.8%.

3.2 Verification of non-drag force

An air-water flow through a 2-dimensional duct of 0.28 m x 1.6 m was simulated to verify the non-drag force models such as the lift force, wall lubrication force, and turbulence dispersion force.

The geometrical condition for this calculation and the gas volume fraction contours for the steps of the non-drag force implementations are presented in Fig. 9. 24 x 24 cells were used for this calculation. The void fraction and inlet velocity were 0.2 and 0.2 m/sec, respectively. All void fraction contours indicate that the gas volume fractions are uniform at the lower inlet and are developed according to the velocity profiles and exerted force to the high outlet.

The lift force seems to push the gas near a wall into the wall, and the wall lubrication force pushes the gas at the wall into the center region. The turbulence dispersion force is not distinguished in this problem, and the sum of the non-drag force seems to result in a lower gas fraction at the wall, a peak near a wall, and a flat gas fraction in a center region.

The horizontal gas volume fractions at the exit for the step of the non-drag force implementation of Fig. 10 clearly show the effect of each non-drag force and their sum. The void fraction without non-drag forces is distributed nearly uniform over the perpendicular direction to the primary flow. The lift force pushed the vapor bubble toward the wall. An increase in the void fraction was observed in the near wall region, which is driven by the large liquid velocity gradient at the near wall.

We must note that the magnitude of the lift force is proportional to the volume fraction of the dispersed vapor fraction, the relative velocity between the liquid and vapor, and the velocity gradient of the continuous phase, and that the direction of this force is dependent upon the bubble diameter.

The lubrication force expelled the gas at the near wall into the central region by a force pushing the liquid into the wall. The volume fraction of the dispersed vapor phase, phasic relative velocity, bubble diameter, distance from the wall, and velocity gradient of the continuous liquid phase are related to this wall lubrication force. This wall lubrication force is known to have just one direction independent of the bubble diameter.

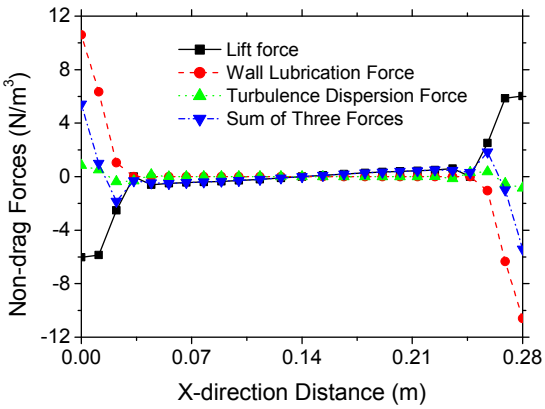

Fig. 11 Non-drag force distribution

The turbulence dispersion force is functioned by the volume fraction gradient of the continuous liquid phase and turbulent kinetic energy. The direction of this turbulence dispersion force is the same as the continuous phase gradient: from a region with a large volume fraction to a region with a small volume fraction.

The combination of the lift force and wall lubrication force make the gas fraction peaked at the near wall. The volume fraction of the dispersed gas fraction in the central region and at the very near wall is relatively lower than that at the gas peaking region.

Non-drag force distributions at the exit are presented in Fig. 11: the lift force, wall lubrication force, turbulence dispersion force, and sum of three forces. The signs of lift force are minus and plus at the left wall and right wall, respectively. This indicates that the lift force acts toward both walls. Wall lubrication forces are plus and minus at the left wall and right wall, respectively, which indicates that the wall lubrication force acts toward the center region. Turbulence dispersion forces do not act in the flat void fraction regions.

The signs of the sum of these three forces follows the dominant force at each region: wall lubrication at the wall, lift force near the wall, and turbulence dispersion force in the void peak region.

4. Conclusions

A computational multi-fluid dynamics (CMFD) code, CUPID, has been developed for realistic simulations of transient two-phase flows in light water nuclear reactor components. In this paper, the implementations and verification calculations of turbulence and non-drag force models were introduced and discussed.

The implementation of the $k-\varepsilon$ turbulence model were verified using a vertical single phase flow. The velocity distribution for this calculation indicates that the $k-\varepsilon$ turbulence models were implemented properly. The implementation of non-drag forces such as the lift force, wall lubrication force, and turbulence dispersion force were then verified based upon a $k-\varepsilon$ turbulence model using an air-water flow through a 2 dimensional duct. The gas volume fraction contours and horizontal gas volume fraction distributions show that each force and the sum of all 3 forces were implemented properly and worked effectively.

Validation calculations for air-water flow tests and subcooled boiling water flow tests will be discussed in the future. It must be noted that the interfacial area transport equation and the wall boiling model should be implemented in the code and assessed before simulating the adiabatic flows and the boiling water flows.

Acknowledgments

This work was supported by the National Research Foundation of Korea (NRF) grant funded by the Korea government (MSIP) (Grant code: 2012M2A8A4025647).

References

[1] 2010, Jeong, J.J., Yoon, H.Y., Park, I.K., Cho, H.K. and Lee, H.D., "Development and Preliminary Assessment of a Three Dimensional Thermal Hydraulics Code, CUPID," *Nuclear Engineering and Technology*, Vol.42, No.3, pp.279-296.

[2] 2010, Jeong, J.J., Yoon, H.Y., Park, I.K. and Cho, H.K., "The CUPID code development and assessment strategy," *Nuclear Engineering and Technology*, 42(6), pp.636-655.

[3] 2012, Yoon, H.Y., Cho, H.K., Lee, J.R., Park, I.K. and Jeong, J.J., "Multi-Scale Thermal-Hydraulic Analysis of PWRs using the CUPID Code," *Nuclear Engineering and Technology*, Vol.44, No.8, pp.831-846.

[4] 2001, The RELAP5-3D Code Development Team, RELAP5-3D© Code Manual Volume I: Code Structure, *System Models and Solution Methods*, Idaho National Engineering and Environmental Laboratory.

[5] 2006, Rhie, C.M. and Chow, W.L., "Numerical Study of the Turbulent Flow Past an Airfoil with Trailing

Edge Separation," *AIAA Journal*, Vol.21, No.11, pp.1525-1532.
[6] 2006, Isshii, M. and Hibiki, T., *Thermo-Fluid Dynamics of Two-Phase Flow*, Chapter 12, Springer, pp.301-336.
[7] 2006, Isshii, M. and Hibiki, T., *Thermo-Fluid Dynamics of Two-Phase Flow*, Chapter 12, Springer, pp.155-169.
[8] Launder, B.E. and Spalding, D.B., "The Numerical Computation of Turbulent Flows," *Computer Methods in Applied Mechanistic and Engineering*, Vol.3, No.2, pp.269-289.
[9] 1965, Saffman, P.G., "The Lift on a Small Sphere in a Slow Shear Flow," *J. Fluid Mechanics*, Vol.22, pp.385-400.
[10] 1980, Zun, I., "The Transverse Migration of Bubbles Influenced by Walls in Vertical Bubbly Flow," *International Journal on Multiphase Flow*, Vol.6, pp. 583-588.
[11] 2002, Tomiyama, A., Tamia, H., Zun, I. and Hosokawa, S., "Transverse Migration of Single Bubbles in Simple Shear Flows," *Chemical Engineering Science*, Vol.57, pp.1849-1858.
[12] 1998, Tomiyama, A., "Struggle with Computational Bubble Dynamics," *Proc. : Third International Conference on Multiphase Flow, ICMF'98*, Lyon, France.
[13] 1966, Wellek, R.M., Agrawal, A.K. and Skelland, A.H.P., "Shapes of Liquid Drops Moving in Liquid Media," *A.I.Ch.E. Journal*, Vol.12, pp.854-862.
[14] 1991, Antal, S.P., Lahey, R.T. and Flaherty, J.E., "Analysis of Phase distribution in Fully developed Laminar Bubbly Two-Phase Flow," *Internaitonal Journal of Multiphase Flow*, Vol.7, pp.635-652.
[15] 1993, Lahey, R.T., Lopez de Bertodano, M. and Jones, O.C., "Phase Distribution in Complex Geomertry Conduits," *Nuclear Engineering and Design*, Vol.141, pp.177-201.
[16] 1992, Lopez de Bertodano, M., *Turbulent Bubbly Two-Phase Flow in a Triangular Duct, PhD Thesis*, Rensselaer Polytechnic Institute, Troy, NY, USA.
[17] 1998, Lopez de Bertodano, M., "Two Fluid Model for Two-Phase Turbulent Jets," *Nuclear Engineering and Design*, Vol.179, pp.65-74.
[18] 1992, Gosman, A.D., Lekakou, C., Politis, S., Issa, R.I. and Looney, M.K., "Multidimensional modeling of turbulent Two Phase Flow in Stirred Vessels," *A.I.Ch.E. Journal*, Vol.38, pp.1946-1956.
[19] 2004, Burns, A.D., Frank, T., Hamill, I. and Shi, J.M., "The Favre Averaged Drag Model for Turbulence Dispersion in Eulerian Multiphase Flow," *ICMF'04*, Yokohama, Japan, Paper 393.
[20] 1998, White, F.M., *Fluid Mechanics, Fourth Edition*, WCB McGraw-Hill, p.349.